Vehicle Positioning Based on Velocity and Heading Angle Observer Using Low-Cost Sensor Fusion

Article *in* Journal of Dynamic Systems Measurement and Control · May 2017

DOI: 10.1115/1.4036881

3 authors, including:

gi seo Park
Korea Advanced Institute of Science and Technology
10 PUBLICATIONS **22** CITATIONS
SEE PROFILE

Seibum Choi
Korea Advanced Institute of Science and Technology
104 PUBLICATIONS **1,088** CITATIONS
SEE PROFILE

Vehicle positioning based on velocity and heading angle observer using low-cost sensor fusion

Giseo Park
Department of Mechanical Engineering, KAIST
KAIST, 291 Daehak-ro, Yuseong-gu, Daejeon 34141, Republic of Korea
giseo123@kaist.ac.kr

Yoonjin Hwang
Department of Mechanical Engineering, KAIST
KAIST, 291 Daehak-ro, Yuseong-gu, Daejeon 34141, Republic of Korea
yoonjinh@kaist.ac.kr

Seibum B. Choi[1]
Professor
Department of Mechanical Engineering, KAIST
KAIST, 291 Daehak-ro, Yuseong-gu, Daejeon 34141, Republic of Korea
sbchoi@kaist.ac.kr
ASME Member

ABSTRACT

The vehicle positioning system can be utilized for various automotive applications. Primarily focusing on practicality, this paper presents a new method for vehicle positioning systems using low-cost sensor fusion, which combines global positioning system (GPS) data and data from easily available in-vehicle sensors. As part of the vehicle positioning, a novel nonlinear observer for vehicle velocity and heading angle estimation is designed, and the convergence of estimation error is also investigated using Lyapunov stability analysis. Based on this estimation information, a new adaptive Kalman filter with rule-based logic provides robust and highly accurate estimations of the vehicle position. It adjusts the noise covariance matrices Q and R in order to adapt to various environments, such as different driving maneuvers and ever-changing GPS conditions. The performance of the entire system is verified through experimental results

[1] Corresponding author.

using a commercial vehicle. Finally, through a comparative study, the effectiveness of the proposed algorithm is confirmed.

Keywords: Sensor fusion, vehicle positioning, state estimation, stability analysis, adaptive Kalman filter.

1 INTRODUCTION

In recent years, vehicle positioning systems have been developed for intelligent transportation systems (ITSs), automatic vehicle applications, and advanced driver assistance systems (ADASs) [1]. In particular, some ADAS applications, such as electronic toll collection, intersection collision warnings, and road curve speed warnings have significant relevance to the vehicle positioning systems [1,2]. Notably, the global positioning system (GPS) has become a widespread sensor for most outdoor land navigation [3]. However, a standard commercial GPS is too problematic to be used in some GPS outage conditions, e.g. urban areas, tunnels and other harsh environments [4]. In addition, temporary loss of the GPS measurement in a congested crossroad caused by a low sampling rate and inaccurate GPS signals can severely affect the driver. In order to achieve an accurate, uninterrupted, and reliable vehicle positioning system, many researchers and industry experts have developed integrated GPSs aided by other sensors [3,4]. In particular, an inertial navigation system (INS) is considered to be a common solution due to its relatively high sampling rate and accuracy; however, it requires additional costs [2]. In contrast, in-vehicle sensors that are installed by default in modern production cars have advantages in terms of cost, which is an important factor for commercialization. The general in-vehicle sensors include the wheel speed sensor, yaw rate sensor, and accelerometer. The combination of GPS and in-vehicle

sensors has already been utilized for vehicle chassis control systems, such as lane keeping and electronic stability control (ESC): it is also suitable for automotive applications [5].

Thus far, various approaches to vehicle positioning based on sensor fusion have been proposed. Yang et al. [7] attempted to utilize fuzzy logic techniques for the dead reckoning of the GPS. To optimize this fuzzy membership function, a genetic algorithm was used. However, a large amount of empirical knowledge for fuzzy logic might involve large computational burdens. Fiengo et al. [8] designed a hybrid localization system that combines Kalman filter with an open loop system. Depending on the conditions, this algorithm can switch between the two strategies. However, due to the absence of vehicle acceleration information having a high sampling rate, the estimated vehicle position has a sampling rate that is too slow for use in vehicle chassis control systems and ITS applications. Bonnabel [9] proposed a low-cost vehicle localization system with a well-chosen nonlinear structure and presented its guaranteed convergence properties. However, in contrast with the Kalman filter algorithm, optimization of some tuning gains in this localization system was not mentioned. Also, the experiments were only performed in low speed conditions under 10 km/h. Some studies have used a vehicle lateral dynamic model to complement the previous algorithms only based on kinematic models [2,4]; however, the uncertain parameters, e.g. vehicle mass, inertia of moment for the yaw axis, and tire cornering stiffness, might cause the accuracy of this vehicle dynamic model to deteriorate. Furthermore, the addition of the vehicle dynamic model can lead to complicated architectures and computational burdens. Therefore, the

primary purpose of this study is to develop the vehicle positioning algorithm considering its practicality for commercialization. A flow chart of the vehicle positioning system is illustrated in Fig. 1.

In this paper, the vehicle velocity and heading angle observer that combine the GPS data with data from in-vehicle sensors is introduced; this is a novel scheme that uses the symmetrical features of the vehicle kinematic model. A new algorithm combining the adaptive Kalman filter (proposed by Mehra [21]) with the rule-based logic is applied to the vehicle positioning. According to the various environments, this algorithm adjusts the noise covariance matrices, and thus induces a highly accurate estimation performance.

This paper is composed of six sections. Section 2 describes the sensors and vehicle kinematic model. Section 3 presents the velocity and heading angle observer with stability analysis. Then, Sec. 4 focuses on the new adaptive Kalman filter with a rule-based logic for the vehicle positioning. In Sec. 5, the proposed algorithms are validated through experiments, and a comparative study is conducted. Finally, Sec. 6 concludes the paper.

2 Sensors and Vehicle Model

2.1 Sensors.

As discussed above, modern production cars are equipped with vehicle control systems, such as antilock braking systems (ABS) and ESC systems, that provide the wheel speed v_w, yaw rate r, longitudinal acceleration a_x and lateral acceleration a_y at the vehicle center of gravity (CG) which are shared by the vehicle controller area network

(CAN). Thus, in order to develop the vehicle positioning algorithm, these sensor data can be easily utilized. For a front-wheel drive vehicle, the average of the speeds of the undriven rear wheels is regarded as the vehicle longitudinal velocity v_x [2,4,6,10,11]. These wheel speed values are filtered through both rate limiter and low pass filter.

$$v_x = g(v_w) = \frac{v_{w,RL} + v_{w,RR}}{2} \tag{1}$$

Since the offset errors of the accelerometer and gyroscope might invoke signal drift issues, a high pass filter or a sensor zeroing algorithm [6] are used to compensate the signals of these sensors.

Low-cost GPS receivers are available in a cost-effective price range. Among them, the MiniGmouse from AscenKorea, Inc. is the GPS receiver used in this study. Table 1 provides the specifications of the GPS. The outputs of GPS are as follows.

1) Latitude p_{lat} and longitude p_{long} in the world geodetic system (WGS-84 standard): These can be converted into Earth-fixed frames in the North-East (NE) global coordinates [8], as follows:

$$p_{n,GPS} = k_{lat}(p_{lat} - p_{o,lat}) \tag{2}$$

$$p_{e,GPS} = k_{long}(p_{long} - p_{o,long}) \tag{3}$$

where $p_{o,lat}$ and $p_{o,long}$ are the latitude and longitude of the origin, respectively; k_{lat} and k_{long} the constant proportional factors; and $p_{n,GPS}$ and $p_{e,GPS}$ the NE global coordinates.

2) Vehicle speed v_s : This excludes the vertical component (z-axis) of velocity.

3) Course angle υ: This denotes the direction of the velocity vector in NE global coordinates. In order that this value is expressed in the vehicle body coordinates, the transformation of the course angle is performed (see Fig. 2). As a result, the range from 0 to 360 deg is transformed into the range from -270 to 90 deg ($\nu_{new} = 90 - \nu$). Both vehicle speed and course angle are measured using the GPS Doppler shifts and the line of sight between vehicle and satellites [25, 26].

4) Number of satellites (NS) and horizontal dilution of precision (HDOP): Because these are related to the accuracy of the position measured by the GPS, a GPS failure can be detected by changes in their values [4,12].

2.2 Vehicle model.

Figure 3 presents the vehicle kinematic model with both vehicle body coordinates for the in-vehicle sensors and NE global coordinates for GPS. This two-dimensional planar model is used to estimate the vehicle velocity and heading angle. It is assumed that the vertical motion of the vehicle is negligible.

Note that the subscripts denote their corresponding coordinates. v_y is the vehicle lateral velocity. r and ψ are the vehicle yaw rate and heading angle (i.e. yaw angle), respectively. The equations of the vehicle model are expressed as follows [13].

$$\dot{p}_e = v_x \cos(\psi) - v_y \sin(\psi) \tag{4}$$

$$\dot{p}_n = v_x \sin(\psi) + v_y \cos(\psi) \tag{5}$$

$$\dot{v}_x = r v_y + a_x \tag{6}$$

$$\dot{v}_y = -r v_x + a_y \tag{7}$$

$$\dot{\psi} = r \tag{8}$$

Furthermore, both the vehicle speed and the course angle measured by GPS can be expressed in the vehicle body coordinates.

$$v_s = \sqrt{v_x^2 + v_y^2} \tag{9}$$

$$\upsilon = \psi + \beta = \psi + tan^{-1}(\frac{v_y}{v_x}) \tag{10}$$

β denotes the side slip angle of the vehicle. Based on Eqs. (3) to (10), a part of the vehicle positioning algorithms, i.e. the vehicle velocity and heading angle observer, is introduced in the following section. Expanding a 2-D vehicle model into a 3-D vehicle model is one of the future studies for robustness to vertical motions on bridges, downhill, and uphill. For example, the estimation algorithm of vehicle roll angle ϕ and pitch angle θ at C.G was developed using an additional sensor, 6-D inertial measurement unit (IMU) which can measure both roll rate p and pitch rate q at C.G by Oh et al. [11]. It is expected that the vertical motion can be considered by combining with these studies: $\dot{v}_x = rv_y + a_x + g\sin\theta$, $\dot{v}_y = -rv_x + a_y + pv_z - g\sin\phi\cos\theta$.

3 Velocity and heading angle observer

The primary purpose of the development of the velocity and heading angle observer is to enhance the weakness of GPS, i.e. the low sampling rate under 10 Hz. Because the low sampling rate of low-cost GPSs is inevitable, GPS measurements v_s and υ might be inaccurate during the vehicle lateral motions on a curved road or at an intersection. The state observer proposed in this section estimates both the velocity and heading angle at a high sampling rate of 100 Hz, which is fast enough to result in the vehicle

positioning being robust to various environments, e.g. curved roads, intersections, and areas with many tall buildings.

3.1 Observer design.

The observer design is based on Eqs. (6) to (8). The state-space expression of the vehicle kinematic model is as follows:

$$\begin{aligned} &\dot{x} = f(x,u) \\ &\begin{bmatrix} \dot{v}_x \\ \dot{v}_y \\ \dot{\psi} \end{bmatrix} = \begin{bmatrix} 0 & r & 0 \\ -r & 0 & 0 \\ 0 & 0 & 0 \end{bmatrix} \begin{bmatrix} v_x \\ v_y \\ \psi \end{bmatrix} + \begin{bmatrix} a_x \\ a_y \\ r \end{bmatrix} \end{aligned} \tag{11}$$

where

$$x = \begin{bmatrix} v_x & v_y & \psi \end{bmatrix}^T, \quad u = \begin{bmatrix} a_x & a_y & r \end{bmatrix}^T.$$

Based on Eqs. (9) and (10), the output equation is as follows:

$$\begin{aligned} &y = h(x) \\ &y = \begin{bmatrix} g(v_w) \\ v_{n,GPS} \\ v_{e,GPS} \end{bmatrix} = \begin{bmatrix} v_x \\ v_s \sin(\nu) \\ v_s \cos(\nu) \end{bmatrix} = \begin{bmatrix} v_x \\ v_x \sin(\psi) + v_y \cos(\psi) \\ v_x \cos(\psi) - v_y \sin(\psi) \end{bmatrix} \end{aligned} \tag{12}$$

where $v_{n,GPS}$ and $v_{e,GPS}$ are the velocity components in the NE global coordinates. Prior to the observer design, the system observability must be checked [14]. Due to the nonlinearity of the output Eq. (12), the observability is locally defined using Lie derivative $L_{\cdot}(\bullet)$ [15,16]. Considering the number of states (x: 3×1 vector), the Lie derivative functions are expressed as follows.

$$\begin{aligned} &L_f^{(0)} = h(x) \\ &L_f^{(k)} = \frac{\partial L_f^{(k-1)}}{\partial x} \cdot \dot{x} = \frac{\partial L_f^{(k-1)}}{\partial x} \cdot f \quad k = 1,2 \end{aligned} \tag{13}$$

The observability function of the system O is derived as follows [15,17]:

$$O = \begin{bmatrix} \frac{\partial L_f^{(0)}}{\partial x} \\ \frac{\partial L_f^{(1)}}{\partial x} \\ \frac{\partial L_f^{(2)}}{\partial x} \end{bmatrix} = \begin{bmatrix} 1 & 0 & 0 \\ \sin(\psi) & \cos(\psi) & v_x\cos(\psi) - v_y\sin(\psi) \\ \cos(\psi) & -\sin(\psi) & -v_x\sin(\psi) - v_y\cos(\psi) \\ 0 & r & 0 \\ 0 & 0 & a_x\cos(\psi) - a_y\sin(\psi) \\ 0 & 0 & -a_x\sin(\psi) - a_y\cos(\psi) \\ -r^2 & 0 & 0 \\ 0 & 0 & -a_x r\sin(\psi) - a_y r\cos(\psi) \\ 0 & 0 & -a_x r\cos(\psi) + a_y r\sin(\psi) \end{bmatrix}. \quad (14)$$

Because O has a full rank of 3, the system including Eqs. (11) and (12) is locally observable at the current state and input [14,15].

The form of nonlinear observer proposed in this section differs from a standard observer form including a simple error feedback term expressed explicitly. The equations of the observer are derived as follows:

$$\begin{aligned} \dot{\hat{v}}_x &= r\hat{v}_y + a_x + L_1(g(v_w) - \hat{v}_x) \\ \dot{\hat{v}}_y &= -r\hat{v}_x + a_y + L_2(v_{n,GPS}\cos(\hat{\psi} + \frac{\hat{v}_y}{v_s}) - v_{e,GPS}\sin(\hat{\psi} + \frac{\hat{v}_y}{v_s})) \\ \dot{\hat{\psi}} &= r + L_2 v_s(v_{n,GPS}\cos(\hat{\psi} + \frac{\hat{v}_y}{v_s}) - v_{e,GPS}\sin(\hat{\psi} + \frac{\hat{v}_y}{v_s})) \end{aligned} \quad (15)$$

where L_1 and L_2 are the positive tuning gains. As described in Eq. (15), the observer possesses the feedback terms using the symmetrical properties of the trigonometrical function. If an extended Kalman filter (EKF) is applied to this system, the high nonlinearity of the output Eq. (12) may deteriorate its performance [18]. From a practical point of view, i.e. the scope of this paper, the proposed nonlinear observer can be a suitable solution because of light computational burden and low structural complexity.

3.2 Stability analysis.

The convergence of the proposed nonlinear observer can be proved by Lyapunov stability analysis. Define $\tilde{v}_x = \hat{v}_x - v_x$, $\tilde{v}_y = \hat{v}_y - v_y$, and $\tilde{\psi} = \hat{\psi} - \psi$. A Lyapunov candidate function V (lower bounded) is defined as follows:

$$V = \frac{1}{2}\tilde{v}_x^{\,2} + \frac{1}{2}\tilde{v}_y^{\,2} + \frac{1}{2}\tilde{\psi}^2 . \tag{16}$$

The time derivative of V is written as follows:

$$\frac{dV}{dt} = \tilde{v}_x\dot{\tilde{v}}_x + \tilde{v}_y\dot{\tilde{v}}_y + \tilde{\psi}\dot{\tilde{\psi}} . \tag{17}$$

Under the assumption that $\tilde{\psi}$, v_y / v_s, and $\hat{v}_y / v_s$ are small enough, the error dynamics of the systems are derived as follows:

$$\dot{\tilde{v}}_x = \dot{\hat{v}}_x - \dot{v}_x = r\tilde{v}_y + L_1(g(v_w) - \hat{v}_x) = r\tilde{v}_y - L_1\tilde{v}_x \tag{18}$$

$$\begin{aligned}
\dot{\tilde{v}}_y &= \dot{\hat{v}}_y - \dot{v}_y = -r\tilde{v}_x + L_2(v_{n,GPS}\cos(\hat{\psi} + \frac{\hat{v}_y}{v_s}) - v_{e,GPS}\sin(\hat{\psi} + \frac{\hat{v}_y}{v_s})) \\
&= -r\tilde{v}_x + L_2(v_s\sin(\psi + \tan^{-1}\frac{v_y}{v_x})\cos(\hat{\psi} + \frac{\hat{v}_y}{v_s}) - v_s\cos(\psi + \tan^{-1}\frac{v_y}{v_x})\sin(\hat{\psi} + \frac{\hat{v}_y}{v_s})) \\
&= -r\tilde{v}_x + L_2 v_s\sin(-\tilde{\psi} + \tan^{-1}\frac{v_y}{v_x} - \frac{\hat{v}_y}{v_s}) \\
&\approx -r\tilde{v}_x + L_2 v_s\sin(-\tilde{\psi}) + L_2 v_s\sin(\tan^{-1}\frac{v_y}{v_x}) + L_2 v_s\sin(-\frac{\hat{v}_y}{v_s}) \\
&= -r\tilde{v}_x - L_2 v_s\tilde{\psi} - L_2\tilde{v}_y
\end{aligned} \tag{19}$$

$$\begin{aligned}
\dot{\tilde{\psi}} &= \dot{\hat{\psi}} - \dot{\psi} = L_2 v_s(v_{n,GPS}\cos(\hat{\psi} + \frac{\hat{v}_y}{v_s}) - v_{e,GPS}\sin(\hat{\psi} + \frac{\hat{v}_y}{v_s})) \\
&= L_2 v_s^{\,2}\sin(-\tilde{\psi} + \tan^{-1}\frac{v_y}{v_x} - \frac{\hat{v}_y}{v_s}) \\
&\approx -L_2 v_s^{\,2}\tilde{\psi} - L_2 v_s\tilde{v}_y
\end{aligned} . \tag{20}$$

By substituting Eqs. (18) to (20) into Eq. (17), the time derivative of V can be expressed as a negative semidefinite function.

$$\begin{aligned}\frac{dV}{dt} &= \tilde{v}_x\dot{\tilde{v}}_x + \tilde{v}_y\dot{\tilde{v}}_y + \tilde{\psi}\dot{\tilde{\psi}} \\ &= \tilde{v}_x(r\tilde{v}_y - L_1\tilde{v}_x) + \tilde{v}_y(-r\tilde{v}_x - L_2 v_s\tilde{\psi} - L_2\tilde{v}_y) + \tilde{\psi}(-L_2 v_s{}^2\tilde{\psi} - L_2 v_s\tilde{v}_y) \\ &= -L_1\tilde{v}_x{}^2 - L_2\tilde{v}_y{}^2 - 2L_2 v_s\tilde{v}_y\tilde{\psi} - L_2 v_s{}^2\tilde{\psi}^2 \\ &= -L_x\tilde{v}_x{}^2 - L_2(\tilde{v}_y + v_s\tilde{\psi})^2 \le 0\end{aligned} \tag{21}$$

In summary, the Lyapunov candidate function $V(\tilde{x},t)$ is decrescent and positive definite. Furthermore, $\dot{V}(\tilde{x},t) \le 0$ for all values of $\tilde{x} \neq 0$, i.e. negative semidefinites. Therefore, the equilibrium point ($\tilde{x}_e = \begin{bmatrix}\tilde{v}_x & \tilde{v}_y & \tilde{\psi}\end{bmatrix}^T = 0$) is Lyapunov stable [19]. This implies that if $\|\tilde{x}(t_0) - \tilde{x}_e\| < \delta$, $\|\tilde{x}(t) - \tilde{x}_e\| < \varepsilon$ for every $t \ge t_0$. Here, δ and ε are positive constants.

The performance of the nonlinear observer was validated by experiments. The driving tests were conducted using a production vehicle (Hyundai Avante). The vehicle was driven on dry asphalt. The detailed experimental setup is introduced in Sec. 5. As depicted in Fig. 4, v_x, v_y, and ψ are accurately estimated for various vehicle maneuvers including straight driving, cornering, braking, and abrupt lane changes on urban roads. Through these maneuvers, the estimation performance of the proposed observer during both transient and steady states is confirmed.

In addition, the lateral velocity and heading angle errors obtained from the experiments are illustrated in Fig. 5. Assuming that 1) the observer is initiated in the no-slip state, i.e. $v_y(t_0) \approx 0$ and $\psi(t_0) \approx \upsilon(t_0)$ (refer to Eq. (10)); 2) also, it is not initiated in the case of harsh GPS condition, e.g. NS<4, the initial errors can be bounded within the small range δ : $\|\tilde{x}(t_0) - \tilde{x}_e\| < \delta$. Thus, using the abovementioned definition of Lyapunov stability, the errors ($\tilde{v}_y$, $\tilde{\psi}$) can be made to be bounded within a constant range ε, as depicted in

Fig. 5. In summary, the advantageous features of the proposed nonlinear observer include the following:

1) The nonlinearity of the tire does not have to be considered.

2) Due to a few tuning gains and simple structures, the procedures for tuning and implementation are simplified.

3) Based on the low-cost sensor fusion, it has a complementary nature, e.g. high sampling rate of the in-vehicle sensors and high accuracy of GPS sensor.

However, in some severe driving maneuvers that can invoke a large amount of roll and pitch motions, other additional logics may assist the proposed observer for more accurate estimations of the velocity and heading angle. However, for the purpose of vehicle positioning, the vehicle velocity and heading angle estimated by the nonlinear observer are sufficiently accurate.

4 **Vehicle positioning**

Kalman filter algorithms that are widely used to optimally estimate a state vector are suitable for estimating vehicle positioning. First, the abovementioned nonlinear observer model is transferred into a discrete model. Then, the vehicle position p_k is approximated using Euler's method for solving a differential equation [2].

$$p_k = p_{k-1} + v_{k-1} T_s \tag{22}$$

where T_s (= 10 ms) is the sampling period of the algorithm. The matrices for the Kalman filter are expressed as follows:

$$\begin{aligned} &x_k = [p_{e,k} \quad p_{n,k}]^T, \quad z_k = [p_{e-GPS,k} \quad p_{n-GPS,k}]^T \\ &F = I_{2\times 2}, \quad H = I_{2\times 2}, \quad Gu_k = [\hat{v}_{e,k-1} T_s \quad \hat{v}_{n,k-1} T_s]^T \end{aligned} \tag{23}$$

where x_k is the state vector; z_k the observation vector; F the transition matrix; H the observation matrix; and Gu_k the input vector. Q and R are the covariance matrices of process noise w_k and measurement noise v_k, respectively. In general, the Kalman filter consists of two steps: a prediction step and an update step (see Fig. 6). In the prediction step of Kalman filtering, to determine the predicted state vector $\hat{x}_k^-$, the velocity and heading angle estimated by the nonlinear observer in Eq. (15) is utilized. Therefore, the velocity models in NE global coordinates are derived as follows.

$$\hat{v}_e = \hat{v}_x \cos(\hat{\psi}) - \hat{v}_y \sin(\hat{\psi}) \tag{24}$$

$$\hat{v}_n = \hat{v}_x \sin(\hat{\psi}) + \hat{v}_y \cos(\hat{\psi}) \tag{25}$$

The predicted error covariance matrix P_k^- is computed simultaneously. In the update step of the Kalman filtering, the Kalman gain K_k is computed, which determines the update weighting between z_k directly measured by GPS and $\hat{x}_k^-$ based on the velocity model [20]. Lastly, the estimated state vector and error covariance at the time step k, i.e. $\hat{x}_k$ and P_k, are obtained.

4.1 Adaptive Kalman filter.

The estimation performance of Kalman filter depends on the reliability of the system modeling and measurement. The system process noise and measurement noise, which are uncorrelated white sequences with zero-means, have the covariance matrices Q and R, respectively. The Q and R in conventional Kalman filter are based primarily on empirical analysis, and are set to a constant for the simplicity of computation [7]. This inflexibility of Q and R might lead performance degradation in the worst-case scenario

[23]. Therefore, for generic applications across a wider range of environments, an adaptive Kalman filtering technique provides online estimations of Q and R based on online stochastic modeling [20-23].

First, the online estimation of R can be derived with the following procedures. The residual sequence is defined as follows:

$$\varepsilon_k = z_k - H\hat{x}_k = z_k - H(\hat{x}_k^- + K_k d_k) = (I - HK_k)d_k \tag{26}$$

where

$$\text{innovation: } d_k = z_k - H\hat{x}_k^- .$$

Taking the variances on both sides of Eq. (26), the theoretical covariance of the residual at the time step k is expressed as follows (the mathematical proof for Eq. (27) is presented in an Appendix):

$$E\{\varepsilon_k \varepsilon_k^T\} = R_k - HP_kH^T . \tag{27}$$

In practice, $E\{\varepsilon_k \varepsilon_k^T\}$ can be obtained through averaging over a moving window of an appropriate size m (= 20). Thus, based on the previous residual sequences, the covariance of the measurement noise can be adopted:

$$\hat{R}_k = \frac{1}{m}\sum_{i=1}^{m} \varepsilon_{k-i}\varepsilon_{k-i}^T + HP_kH^T . \tag{28}$$

Because the simultaneous online estimation of Q and R can cause the filter to diverge [20], the covariance matrix Q is regarded as a nominal value during the online estimation of R. In advance, the open-loop system was implemented and then, its process noises were computed. The average of covariance matrices of process noises, $\frac{1}{n}\sum_{k=1}^{n} Q_k$ is regarded as the nominal value.

Next, in order to obtain the online estimation of Q, a scaling method is used [20,23]. The abovementioned innovation term is rewritten as follows:

$$d_k = H(x_k - \hat{x}_k^-) + \mathrm{v}_k \,. \tag{29}$$

As conducted earlier, taking the variances on both sides of Eq. (29), the theoretical covariance of the innovation term is given as follows:

$$E\{d_k d_k^T\} = HP_k^- H^T + R_k \,. \tag{30}$$

The average over the moving window of size m is substituted for $E\{d_k d_k^T\}$; thus, the theoretical P_k^- is changed into an estimated $\hat{P}_k^-$. During the online estimation of Q, R is set to a nominal value.

$$\frac{1}{m}\sum_{i=1}^{m} d_{k-i} d_{k-i}^T = H\hat{P}_k^- H^T + R_k \tag{31}$$

In order to follow the estimated $\hat{P}_k^-$, a simple and intuitive scaling method is utilized [23]. As described in Eq. (32), the scaling factor α denotes an approximation ratio between the estimated $\hat{P}_k^-$ and the theoretical P_k^-:

$$\hat{Q}_k = Q_{k-1}\sqrt{\alpha} \tag{32}$$

where

$$\alpha = \frac{trace\{H\hat{P}_k^- H^T\}}{trace\{HP_k^- H^T\}} = \frac{trace\{\frac{1}{m}\sum_{i=1}^{m} d_{k-i} d_{k-i}^T - R_k\}}{trace\{HP_k^- H^T\}} \,. \\ = \frac{trace\{H(FP_{k-1}F^T + \tilde{Q}_{k-1})H^T\}}{trace\{H(FP_{k-1}F^T + Q_{k-1})H^T\}}$$

In order to add a smoothing effect, the scaling factor is set to a value near 1. Therefore, a square root is applied to the scale factor in Eq. (32) [23]. The range of $\hat{Q}$ has to be limited in order to prevent divergence issues. Although this scaling method does not

directly resolve $\hat{P}_k^-$, it is sufficiently effective due to the scaling factor, which makes the estimated $\hat{P}_k^-$ follow the theoretical P_k^-. The effectiveness of the adaptive Kalman filter is validated in the following section.

4.2 Rule-based logic for Kalman gain.

The Kalman gain based on the online estimation of noise covariance relies on rule-based logic using GPS measurements, such as NS and HDOP. As discussed above, the outage of GPS signals can be detected in real time using these values. For a low NS below a constant threshold NS_{low} (= 5) or high HDOP above a threshold $HDOP_{up}$ (= 5), the P_{e-GPS} and P_{n-GPS} directly measured by GPS are regarded as unavailable data; thus, an open-loop estimator without correction terms has been used [2,4]. Otherwise, it is probable that high NS above a threshold NS_{up} (= 10) or low HDOP below a threshold $HDOP_{low}$ (= 1) corresponds to highly accurate GPS measurements z_k. In this case, the online estimation of R (28), which reflects the changes of R in real time more quickly than the online estimation of Q in Eq. (32), is implemented using a rule-based logic. In the other situations (i.e. normal GPS conditions), the online estimation of Q, which is less sensitive to the excessive noises of GPS position measurements due to the smoothing effect, is adopted [20]. The smoothly varying equation (32) is considered more suitable for a long time in normal GPS condition. The overall rule-based logics for Kalman gain are summarized in Table 2. In the case of extremely harsh GPS conditions such as tunnels (NS=0), the vehicle position has to be estimated by direct integration of the velocity without GPS signals [9]. Figure 7 depicts the number of satellites in use, the horizontal dilution of precision, and the Euclidean distance errors between the position

measured by GPS and the reference obtained by RT3100. This RT3100 from Oxford Technical Solutions Ltd. is a highly accurate differential GPS (DGPS)-based vehicle localization system. The Euclidean distance error between two points p and q is defined as follows.

$$d(p,q) = d(q,p) = \sqrt{(q_x - p_x)^2 + (q_y - p_y)^2} \tag{33}$$

As depicted in Fig. 7, the Euclidean distance errors significantly increase in the regions with tall buildings, e.g. GPS outage 1 and GPS outage 2 in Fig. 8. The test drive course is thoroughly explained in the following section. According to the rule-based logic in Algorithm 1, the GPS mode is selected, as depicted in Fig. 9(a): mode 0, 1, and 2 denote the open-loop estimator, online estimation of Q with a nominal R, and online estimation of R with a nominal Q, respectively. Furthermore, each element in the noise covariance matrices Q and R is illustrated in Figs. 9(b) and 9(c). Mode 1 occupies a large portion during the test-drive. Although mode 2 is less frequent than mode 1, mode 2 with a significantly decreasing R can assist the proposed algorithm to maintain high accuracy. The effectiveness of the rule-based logic is validated experimentally in the next section.

5 Experiment

5.1 Experimental setup.

The experimental setup for the verification of the proposed algorithm is presented in Fig. 10. A low-cost GPS receiver (MiniGmouse from AscenKorea, Inc.) and DGPS antenna of RT3100 (for verification purposes) were installed on the roof of the vehicle. Assuming that RT3100 is mounted at the CG of the test vehicle (Hyundai Avante), the vertical distance between the GPS and RT3100 was approximately 600 mm. Along with the

vehicle position, the vehicle velocity and heading angle taken by the RT3100 are regarded as the actual values. Through CompactRIO data-logging device from National Instruments, both input and output data are monitored in real time. The sampling period of the in-vehicle sensors and RT3100 was 10 ms, and that of GPS was 100 ms. As mentioned above, the sampling rate of the position estimation algorithm is identical to that of the in-vehicle sensors.

The test drive course was in KAIST campus which represents an urban area; it included several driving conditions, such as straight roads, curves, intersections, and sudden deceleration to avoid collisions. Figure 8 presents a map of the test drive course captured from Google Earth. The trajectories followed by the test vehicle included four turns around KAIST. The overall time for the test was approximately 14 minutes.

5.2 Experimental results.

Prior to the discussion of vehicle positioning test results, the velocity and heading angle estimated by the nonlinear observer are presented in Figs. 11 and 12. Before the vehicle positioning algorithm started, the convergence of the nonlinear observer was checked preferentially. Thus, the first 50 seconds was omitted from the vehicle positioning results in Figs. 7-9, 13-14 and Table 3. As shown in Fig. 11, the vehicle moved at a longitudinal velocity varying from 1 to 12 m/s. Whenever the lateral velocity v_y increased quickly due to steering maneuvers at the curves, it was confirmed that the estimated $\hat{v}_y$ quickly followed the actual values. This implies that the tracking performance was accurate in the transient states too. During the long time period of trajectories (longer than 800 s), the proposed observer exhibited highly accurate

estimation results without drift issues. However, distinct estimation errors of $\hat{v}_y$ was observed at around 650 s due to the unexpectedly inaccurate GPS measurements. In the vehicle positioning, these errors of the nonlinear observer were compensated by adaptive Kalman filtering. In an extreme case of really large initial error which means that the heading angle estimation was initialized far from the actual value, the nonlinear observer converged equally well regardless of its initial values, as depicted in Fig. 12. In fact, these extreme cases occurs rarely.

For the behaviors of adaptive Kalman filter with the rule-based logic, refer to Figs. 7 and 9. Figure 13 presents the reference position obtained from RT-3100 and the estimated value from the proposed vehicle positioning algorithm. In addition, in order to evaluate the performance of the proposed algorithm, it was compared with the values directly measured by the GPS. The detailed data in several environments, such as curves, straight roads, and GPS outages, corresponded with each region in Fig. 8. As shown in the trajectories on the curve 1, the estimated positions were quite close to the actual values, while the GPS measurements had large errors due to its sampling rate being too low to reflect the fast changes of the vehicle lateral motion. As depicted in the trajectories on the straight roads, while the GPS measurements drifted due to the multipath GPS signal problem, the adaptive Kalman filter rejected these errors effectively by attributing more weight to the velocity model than the GPS measurements.

The GPS measurements in GPS outage 1 and GPS outage 2 had irregular trajectories with large amounts of position errors. In contrast, the differences between the

reference and estimated positions were tolerable despite the harsh GPS conditions. Assuming that the width of a general midsize vehicle is approximately 1.6 m and a standard lane width is approximately 3.6 m, the root mean square (RMS) distance error of 1 m is set to the error tolerance limit in this paper. Consequently, the estimation results satisfy this numerical goal.

The Euclidean distance errors during the entire test period are illustrated in Fig. 14. In this figure, five different types of vehicle positioning algorithms are compared: 1) the measurement from the GPS, 2) the conventional KF based on the GPS data, 3) the adaptive KF based on the GPS data, 4) the conventional KF based on the nonlinear observer, and 5) the adaptive KF based on the nonlinear observer, which is the algorithm developed in this paper. The velocity model of the Kalman filters based on GPS data is the velocity components obtained from GPS, i.e. Gu_k, in Eq. (23) is changed into $[v_{e-GPS}T_s \quad v_{n-GPS}T_s]^T$.

As demonstrated in these results, whenever GPS measurement error was close to zero, the online estimation of R was decreased quickly reflecting the accurate GPS measurement. Thus, adaptive Kalman filter can prevent errors from being accumulated. Furthermore, in comparison with conventional Kalman filter, adaptive Kalman filter showed the reduced position error for the entire test period.

For the comparative study, the statistics of the Euclidean distance errors of the different algorithms are presented in Table 3. The results are divided into four data sets, and each data set during one cycle represents both the RMS and maximum errors (note that the data set 4 is for less than one round cycle). The Kalman filter based on the nonlinear

observer had better performance than that based on GPS data throughout all data sets. This tendency was resulted from the sensor fusion integrating GPS and in-vehicle sensors having the advantage of the higher sampling rate than that of just GPS. In accordance with the total RMS errors, only the proposed algorithm (algorithm 5) reached the goals for vehicle positioning, which was an RMS error of less than 1 m. Furthermore, its maximum error of 2.115 m was relatively small, whereas the worst algorithm (algorithm 1) recorded errors of up to 10 m. Due to the trade-off between price and performance of GPS, intrinsic measurement errors in the low-cost GPS is inevitable. Despite this limitation, it was confirmed that the proposed vehicle positioning algorithm can improve the estimation performance significantly, as described in Table 3.

6 **Conclusion**

This study presents a novel method of vehicle positioning comprised of both a nonlinear observer and a new adaptive Kalman filter. The nonlinear observer using low-cost sensor fusion exhibits high accuracy and reliable estimation results in terms of vehicle velocity and heading angle. In addition, due to its simplicity of tuning and implementation, it can be easily applied to production vehicles. The new adaptive Kalman filter with a rule-based logic for Kalman gains provides robust estimation performance in various driving conditions and harsh GPS environments. Adjusting the noise covariance matrices Q and R allows the adaptive Kalman filtering to adapt to these environments effectively. Through the large set of trajectories, the estimation performance of the proposed algorithm was validated to be robust. Furthermore, from

the comparative study with five different algorithms, the effectiveness of the proposed algorithm was confirmed.

In summary, the vehicle positioning algorithm proposed in this paper distinguishes itself from previous studies: 1) it accompanied the velocity and heading angle estimators, which can also be utilized for both ITS applications and vehicle control systems; 2) based on low-cost sensor fusion, it is cost-competitive; and 3) it is a practical solution that can be implemented easily in production vehicles due to the light computational burden, high availability, fast update rate, and reliable estimation performance.

This paper has demonstrated that the proposed adaptive Kalman filter based on a nonlinear observer can make a significant contribution to the development of an accurate vehicle positioning system.

APPENDIX

Proof of Eq. (27) is as follows:

$$S_k = E\{d_k d_k^T\} = HP_k^- H^T + E\{v_k v_k^T\} = HP_k^- H^T + R_k$$
$$K_k = P_k^- H^T S_k^{-1}$$
$$\varepsilon_k = z_k - H(\hat{x}_k^- + K_k d_k) = (I - HK_k)d_k$$

$$E\{\varepsilon_k \varepsilon_k^T\} = (I - HK_k)S_k(I - HK_k)^T$$
$$= (I - HK_k)(HP_k^- H^T + R_k)(I - K_k^T H^T)$$
$$= R_k \underbrace{+HK_k R_k K_k^T H^T + HK_k HP_k^- H^T K_k^T H^T}_{(1)}$$
$$\underbrace{-R_k K_k^T H^T - HP_k^- H^T K_k^T H^T - HK_k HP_k^- H^T - HK_k R_k + HP_k^- H^T}_{(2)}$$
$$= R_k + HK_k HP_k^- H^T - HP_k^- H^T$$
$$= R_k - HP_k H^T$$

$$(1) = HK_k(R_k + HP_k^- H^T)K_k^T H^T = HK_k S_k K_k^T H^T = HK_k HP_k^- H^T$$
$$(2) = -(R_k + HP_k^- H^T)K_k^T H^T - HK_k(HP_k^- H^T + R_k) + HP_k^- H^T$$
$$= -S_k K_k^T H^T - HK_k S_k + HP_k^- H^T = -HP_k^- H^T$$

.

ACKNOWLEDGMENT

This work was supported by the National Research Foundation of Korea(NRF) grant funded by the Korea government(MSIP) (No.2017R1A2B4004116) and the BK21+ program through the NRF funded by the Ministry of Education Korea. This research was supported by the MSIP(Ministry of Science, ICT and Future Planning), Korea, under the ITRC(Information Technology Research Center) support program(ITTP-2017-2012-0-00628) supervised by the ITTP(Institute for Information & communications Technology Promotion).

REFERENCES

[1] Jo, K., Lee, M., and Sunwoo, M., 2016, "Road Slope Aided Vehicle Position Estimation System Based on Sensor Fusion of GPS and Automotive Onboard Sensors," IEEE Trans. Intell. Transport. Syst., **17**(1), pp. 250-263.
[2] Jo, K., Chu, K., and Sunwoo, M., 2012, "Interacting Multiple Model Filter-Based Sensor Fusion of GPS With In-Vehicle Sensors for Real-Time Vehicle Positioning," IEEE Trans. Intell. Transport. Syst., **13**(1), pp. 329-343.
[3] Bevly, D. M., 2004, "Global Positioning System (GPS): A Low-Cost Velocity Sensor for Correcting Inertial Sensor Errors on Ground Vehicles," ASME J. Dyn. Syst., Meas., Control, **126**(2), pp. 255-264.
[4] Li, X., Chen, W., and Chan, C., 2014, "A reliable multisensory fusion strategy for land vehicle positioning using Low cost sensors," IMechE Part D: J Automobile Engineering, **228**(12), pp. 1375-1397.
[5] Wu, Z., Yao, M., Ma, H., and Jia, W., 2013, "Improving Accuracy of the Vehicle Attitude Estimation for Low-Cost INS/GPS Integration Aided by the GPS-Measured Course Angle," IEEE Trans. Intell. Transport. Syst., **14**(2), pp. 553-564.
[6] Oh, J. J., and Choi, S. B., 2012, "Vehicle Velocity Observer Design Using 6-D IMU and Multiple-observer Approach," IEEE Trans. Intell. Transport. Syst., **13**(4), pp. 1865-1879.
[7] Yang, Y., Gu, Z., and Hu, L., 2007, "Research on the information fusion method of the Global Positioning System-Dead reckoning vehicle integrated navigation system," IMechE Part D: J Automobile Engineering, **221**(5), pp. 543-553.
[8] Fiengo, G., Domenico, D. D., and Glielmo, L., 2009, "A hybrid procedure strategy for vehicle localization system: Design and prototyping," Control Engineering Practice, **17**(1), pp. 14-25.

[9] Bonnabel, S., and Salaun, E., 2011, "Design and prototyping of a low-cost vehicle localization system with Guaranteed convergence properties," Control Engineering Practice, **19**(6), pp. 591-601.
[10] Oh, J. J., and Choi, S. B., 2013, "Dynamic sensor zeroing algorithm of 6D IMU mounted on ground vehicles," Int. J. Auto. Technol., **14**(2), pp. 221-231.
[11] Oh, J. J., and Choi, S. B., 2013, "Vehicle roll and pitch angle estimation using a cost-effective six-dimensional inertial measurement unit," IMechE Part D: J Automobile Engineering, **227**(4), pp. 577-590.
[12] Langley, R. B., 1999, "Dilution of Precision," GPS World.
[13] Leung, K. T., Whidborne, J. F., Purdy, D., and Barber, P., 2011, "Road vehicle sate estimation using low-cost GPS/INS," Mech. Sys. and Sig. Process., **25**(6), pp. 1988-2004.
[14] Franklin, G. F., Powell, J. D., and Naeini, A. E., 2005, *Feedback Control of Dynamic Systems, 6th ed.*, Upper Saddle River, NY, USA: Prentice-Hall.
[15] Hermann, R., and Krener, A. J., 1977, "Nonlinear Controllability and Observability," IEEE Trans. Auto. Con., **22**(5), pp. 728-740.
[16] Stephant, J., Charara, A., and Meizel, D., 2007, "Evaluation of a sliding mode observer for vehicle sideslip angle," Control Engineering Practice, **15**(7), pp. 803-812.
[17] Travers, M., and Choset, H., 2015, "Use of the Nonlinear Observability Rank Condition for Improved Parametric Estimation," *Proc*. *IEEE ICRA*, Washington, USA.
[18] Simon, D., 2006, *Optimal State Estimation*, New York: Wiley.
[19] Khalil, H., 2002, *Nonlinear System. 3rd ed.*, Upper Saddle River, NJ, USA: Prentice-Hall.
[20] Almagbile, A., Wang, J., and Ding, W., 2010, "Evaluating the Performances of Adaptive Kalman Filter Methods in GPS/INS Integration," J. Global Positioning Systems, **9**(1), pp. 33-40.
[21] Mehra, R., 1970, "On the identification of variances and adaptive Kalman filtering," IEEE Trans. Auto. Con., **15**(2), pp. 175-184.
[22] Mohamed, A. H., and Schwarz, K. P., 1999, "Adaptive Kalman Filtering for INS/GPS," Journal of Geodesy, **73**(4), pp. 193-203.
[23] Ding, W., Wang, J., and Rizos, C., 2007, "Improving Adaptive Kalman Estimation in GPS/INS Integration," The Journal of Navigation, **60**(3), pp. 517-529.
[24] Yoon, J., and Peng, H., 2014, "A Cost-Effective Sideslip Estimation Method Using Velocity Measurements From Two GPS Receivers," IEEE Trans. Vehi. Technol., **63**(6), pp. 2589-2599.
[25] Meguro, J., Kojima, Y., Suzuki, N., and Teramoto, E., 2012, "Positioning Technique Based on Vehicle Trajectory Using GPS Raw Data and Low-cost IMU," Int. J. Auto. Eng., **3**, pp. 75-80.
[26] Yoon, J. H., Li, S. E. and Ahn, C., 2016, "Estimation of Vehicle Sideslip Angle and Tire-road Friction Coefficient Based on Magnetometer with GPS," Int. J. Auto. Technol., **17**(3), pp. 427-435.
[27] Han, K., Hwang, Y., Lee, E., and Choi, S. B., 2016, "Robust Estimation of Maximum Tire-road Friction Coefficient considering Road Surface Irregularity," Int. J. Auto. Technol., **17**(3), pp. 415-425.

Table caption list

Figure caption list

Parameter	Typical	Unit
TTFF	1	seconds (hot start)
Position error	3	m (50% CEP)
Velocity error	0.1	m/s (RMS)
Sampling rate	10	Hz

TTFF: time to first fix. Hot start: GPS receiver restarts using the values stored in its internal memory. CEP: circular error of probability.

Table 1 GPS specification data

Rule-based Kalman gain

$\hat{x}_k^- = \hat{x}_{k-1} + \hat{v}_{k-1} T_s$

If $NS < NS_{low}$ or $HDOP > HDOP_{up}$ then

$\hat{x}_k = \hat{x}_k^-$

▷ Open loop estimator

Else if $NS > NS_{up}$ or $HDOP < HDOP_{low}$ then

$\hat{R}_k = \frac{1}{m} \sum_{i=1}^{m} \varepsilon_{k-i} \varepsilon_{k-i}^T + H \hat{P}_k H^T$

$\hat{x}_k = \hat{x}_k^- + K_k (z_k - H \hat{x}_k^-)$

▷ Nominal Q and varying R

Else

$\hat{Q}_k = Q_{k-1} \sqrt{\alpha}$

$\hat{x}_k = \hat{x}_k^- + K_k (z_k - H \hat{x}_k^-)$

▷ Nominal R and varying Q

End if

Table 2 Rule-based Kalman gain

Algorithm	Set 1 0~215.3s		Set 2 215.31~441.6s		Set 3 441.61~672.2s		Set 4 672.21~815.24s		Total RMS (m)
	RMS (m)	Max (m)	RMS (m)	Max (m)	RMS (m)	Max (m)	RMS (m)	Max (m)	
1	4.036	10.84	4.215	8.959	3.875	11.39	4.308	10.92	4.091
2	0.865	1.697	1.785	4.229	1.661	2.496	1.632	2.315	1.526
3	0.810	1.648	1.179	2.189	1.402	2.396	1.223	1.743	1.174
4	0.665	1.529	1.692	4.186	1.375	2.138	1.286	2.078	1.318
5	0.655	1.505	1.028	1.709	1.112	2.115	0.867	1.474	0.943

Table 3 Statistics of the Euclidean distance errors of five different algorithms

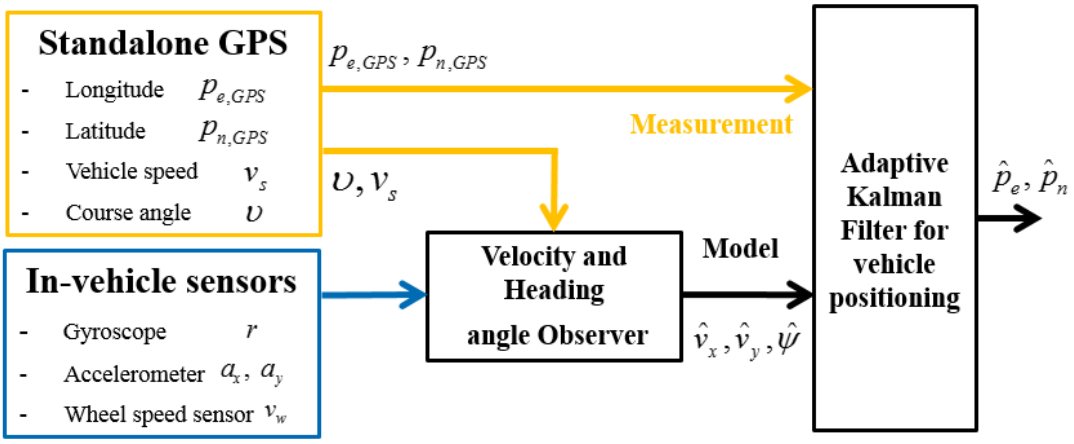

Fig. 1 Flow chart of the proposed vehicle positioning system

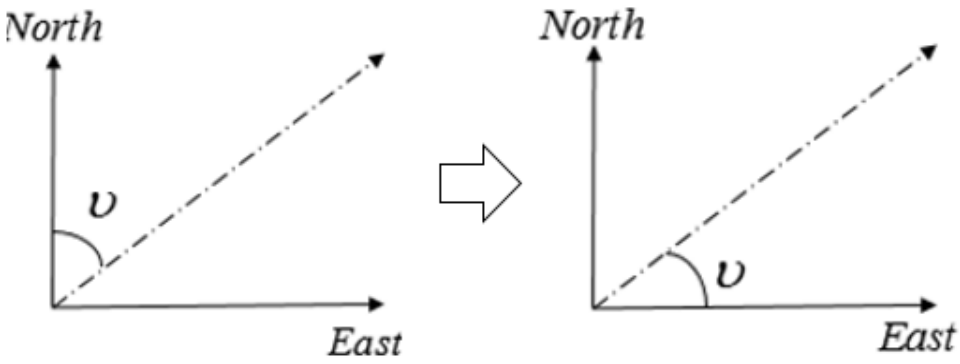

Fig. 2 Transformation of the GPS course angle: from clockwise to counter-clockwise

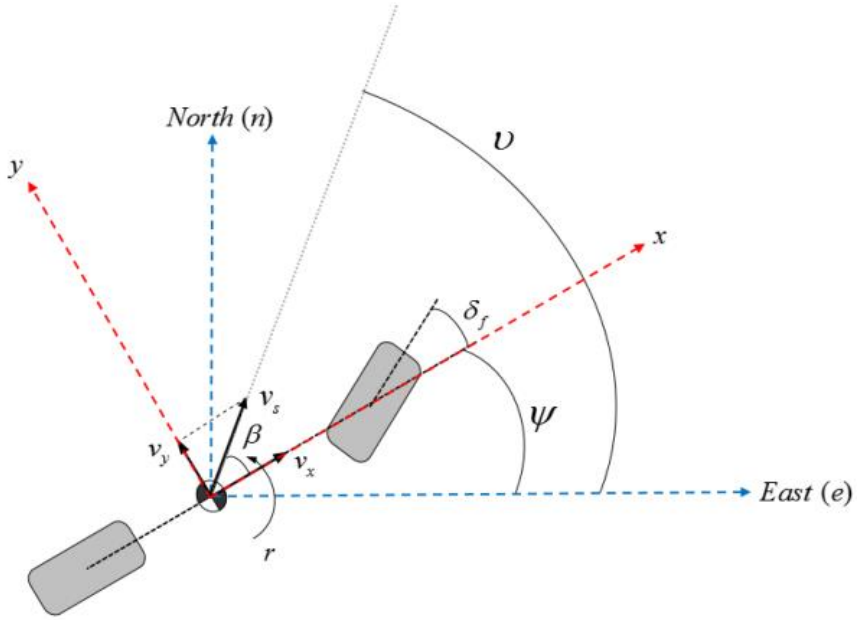

Fig. 3 Vehicle kinematic model

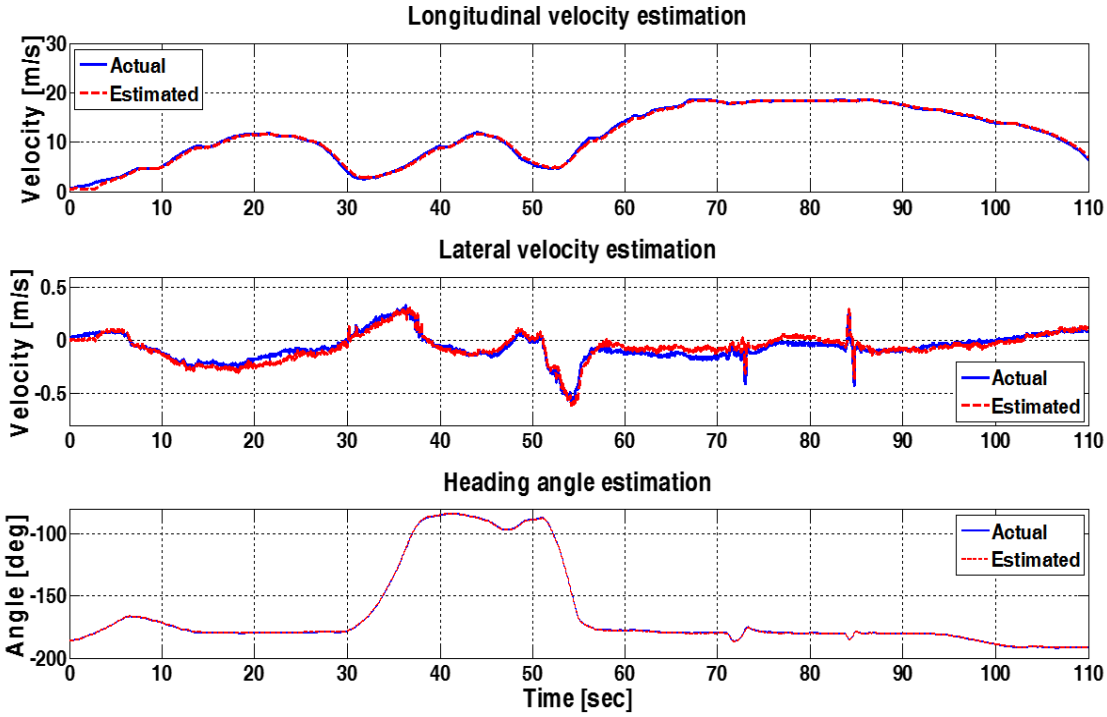

Fig. 4 Estimation results obtained from the nonlinear observer

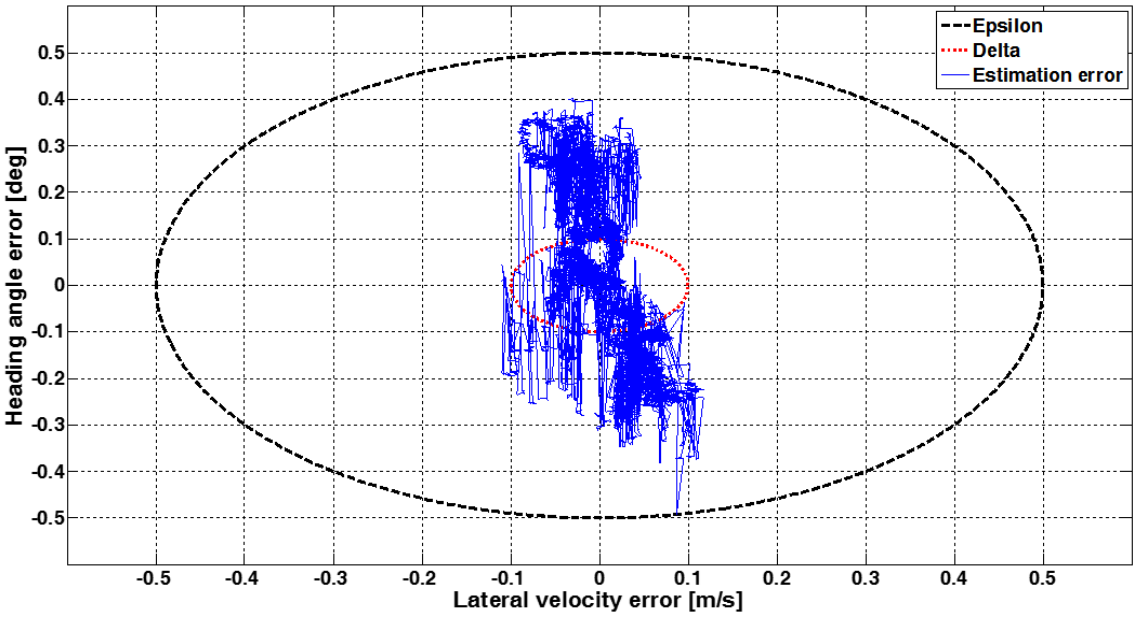

Fig. 5 Illustration of stability

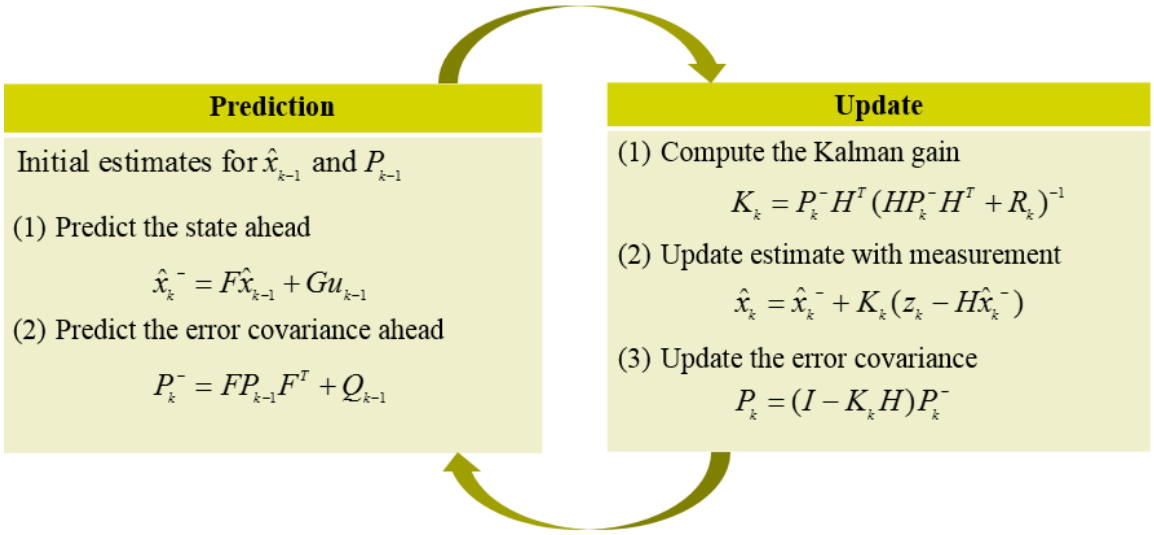

Fig. 6 Kalman filter process

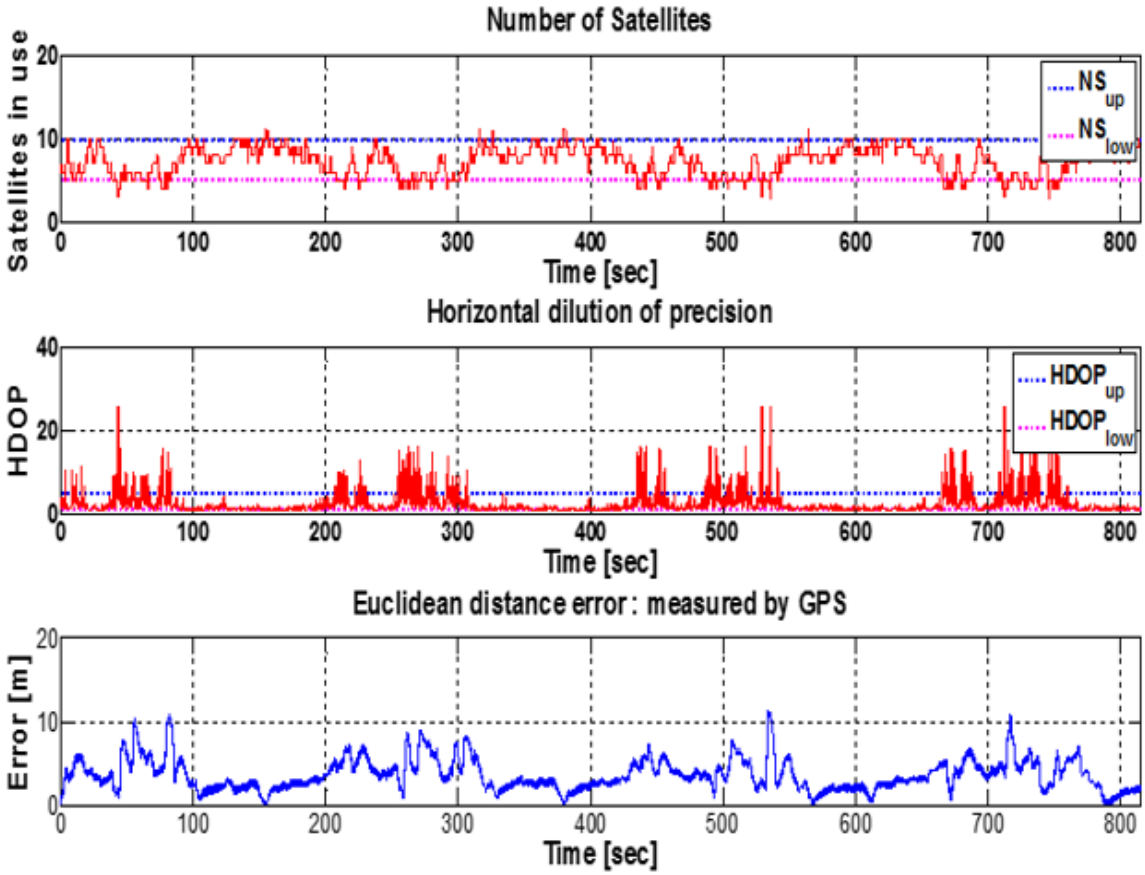

Fig. 7 Number of satellites, HDOP, and measurement error of the GPS

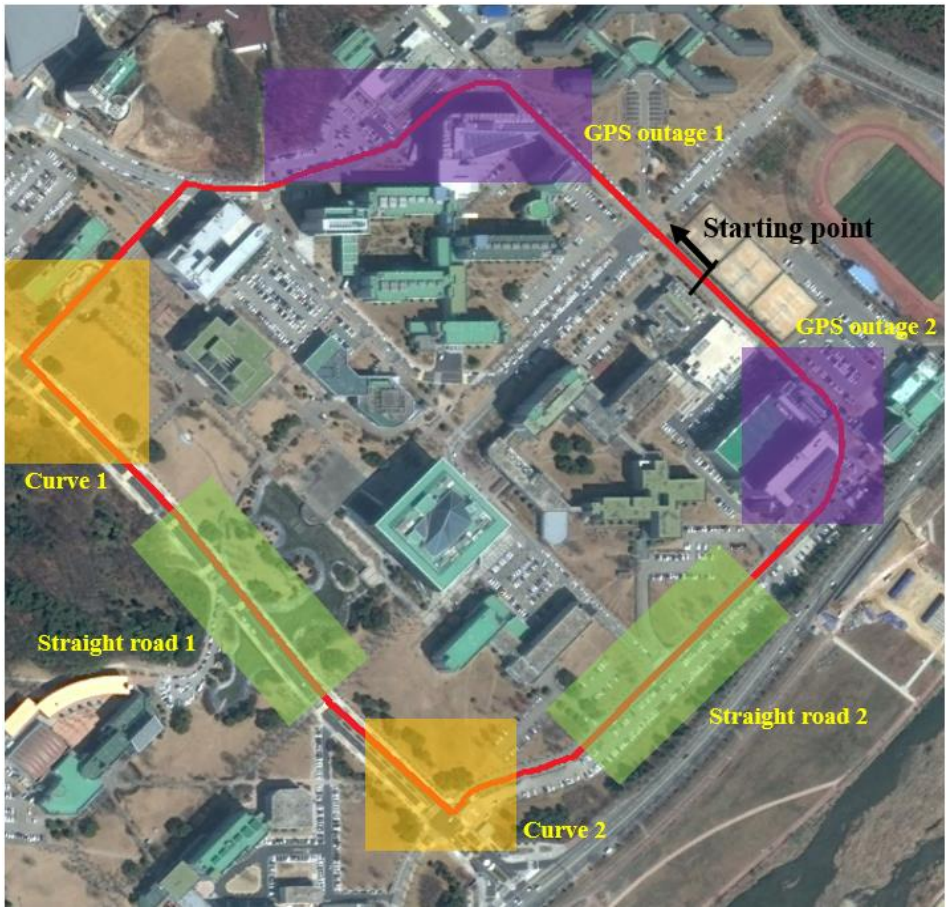

Fig. 8 Test drive course (captured from Google Earth)

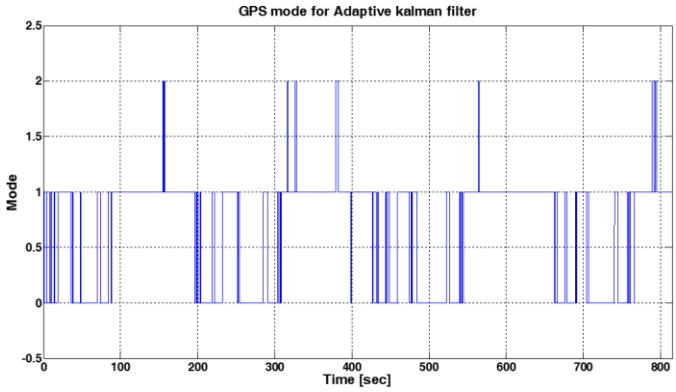

(a)

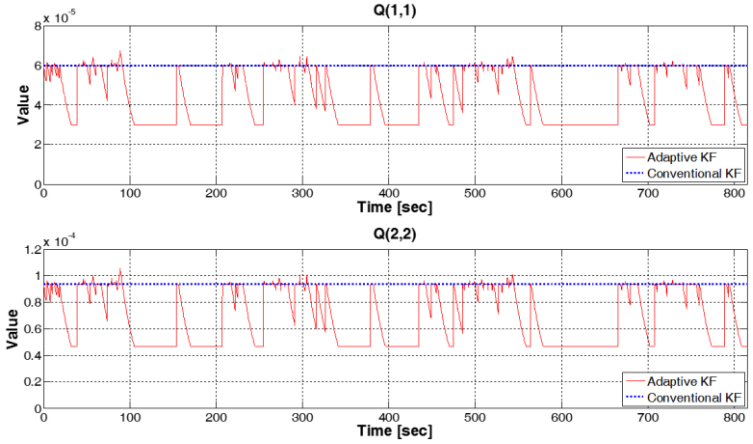

(b)

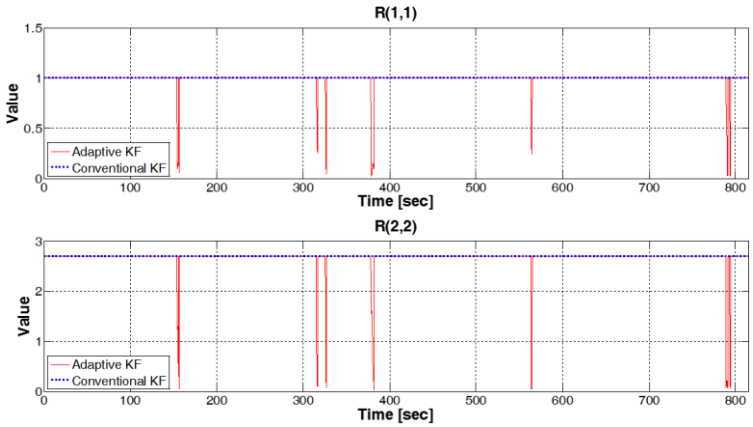

(c)

Fig. 9 Adaptive Kalman filter: (a) GPS mode, (b) online estimation of Q, and (c) online estimation of R

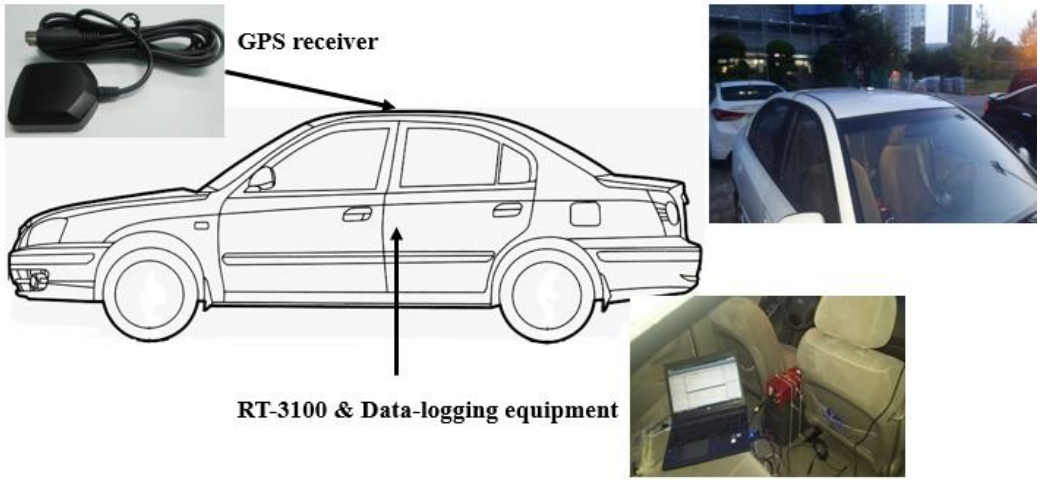

Fig. 10 Experiment setup

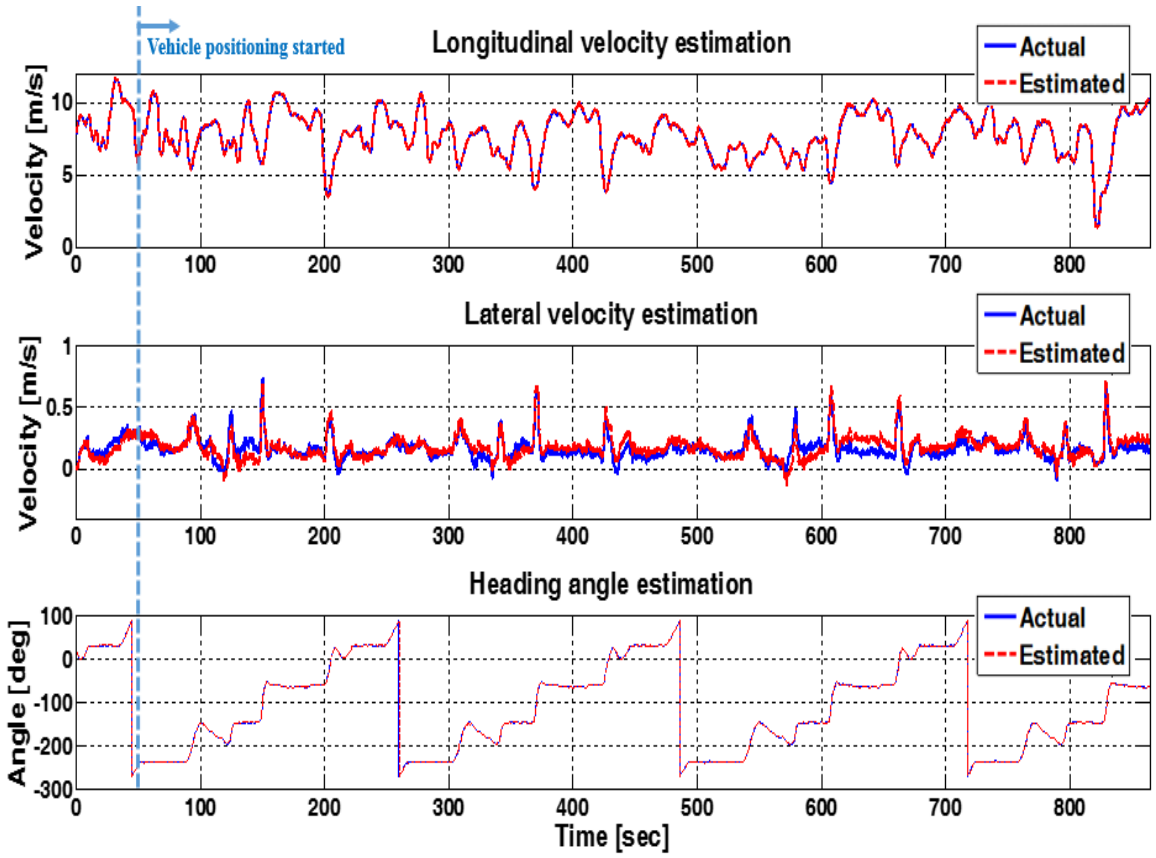

Fig. 11 Velocity and heading angle estimation results

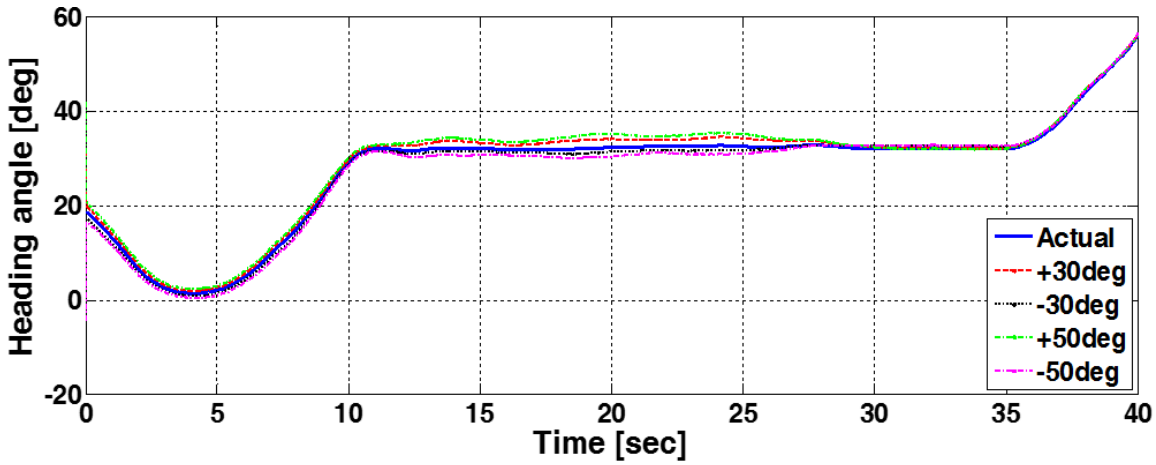

Fig. 12 Heading angle estimation with bad initialization errors

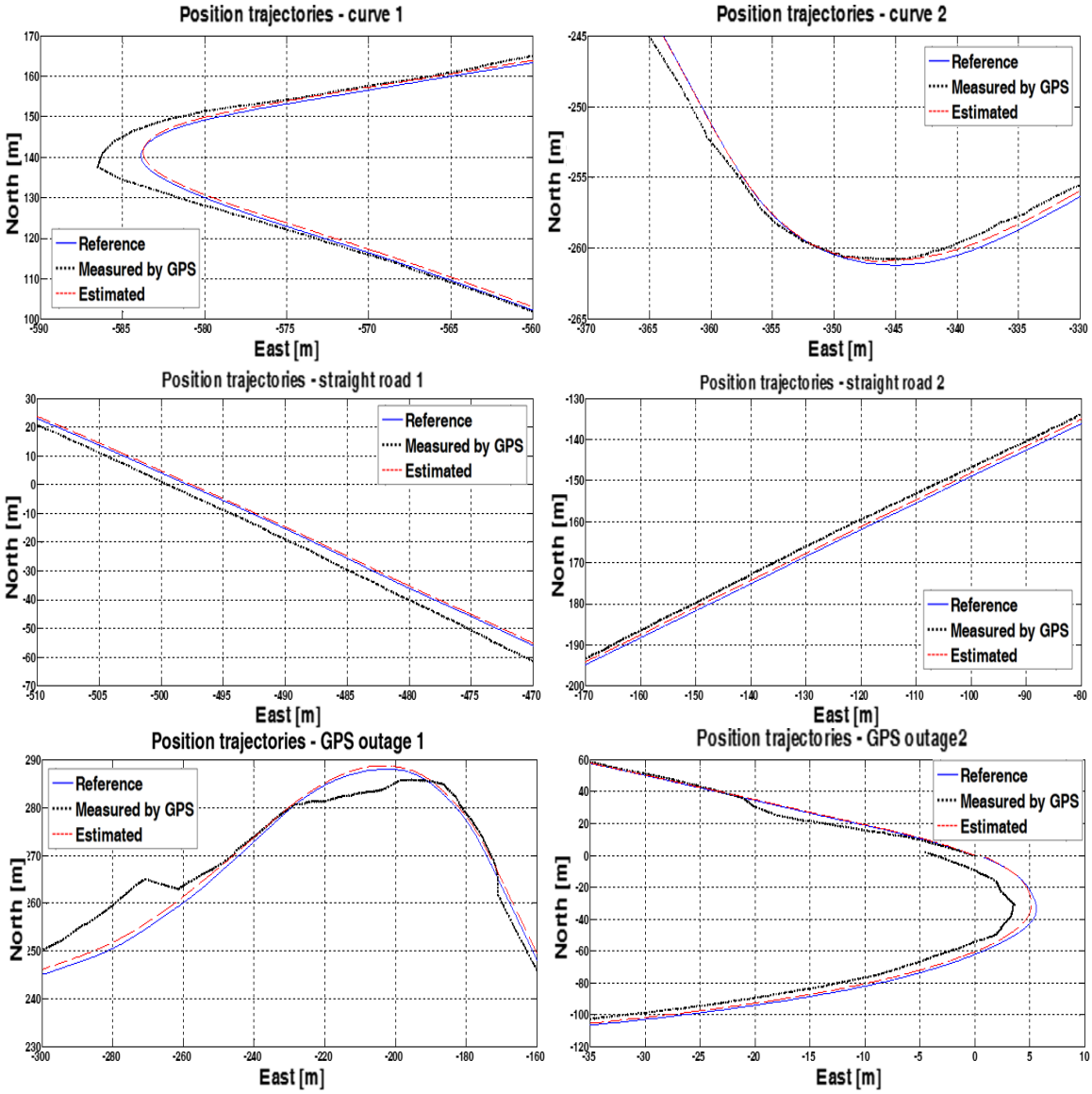

Fig. 13 Vehicle positioning results during one cycle

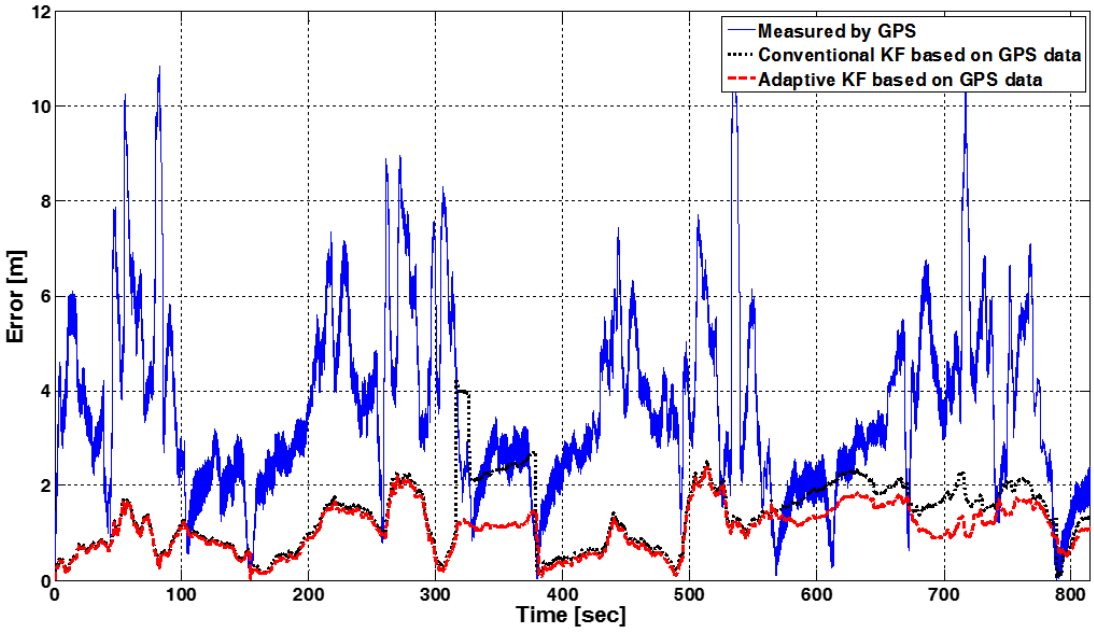

(a)

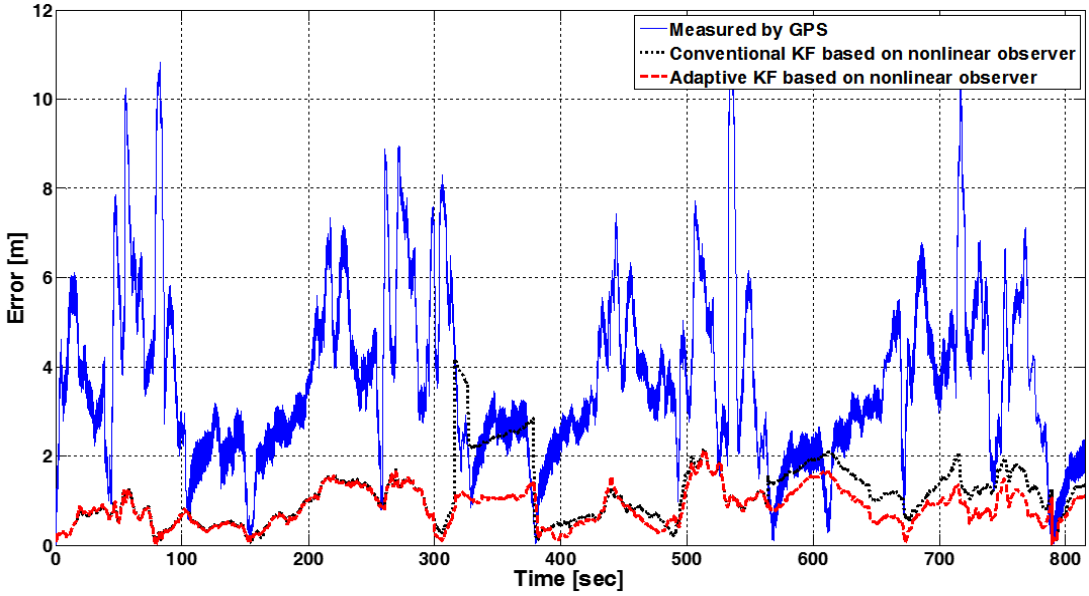

(b)

Fig. 14 Each Euclidean distance error: (a) KFs based on the GPS data and (b) KFs based on the nonlinear observer